A Nonlinear Pilot Model for Hover

Dominick Andrisani II* and Ching-Fu Gau†
Purdue University, West Lafayette, Indiana

This paper deals with persistent oscillations in position and attitude observed in flight on a piloted VTOL during precision hover. Properties of the oscillation are shown to correlate strongly with Cooper-Harper pilot ratings. A simple yet nonlinear pilot model is developed which predicts many of the properties of the pilot-in-the-loop system behavior.

Nomenclature

A,M	= properties of the ideal relay with dead zone ($M=0.25$ in., $A=0.125$ in.)
Configuration 217C	= configuration C of X-22A flight 217
e_X	= error in X position, $=X_c-X$ (ft)
E	= amplitude of sinusoidal input to nonlinear element $N(E)$
K_x	= pilot position error gain (in./ft)
$K_{\dot{x}_c}$	= ratio of steady state x translational velocity per inch of pilot's stick position (ft/s/in.)
K_x^*	= minimum pilot position error gain to maintain a stable limit cycle (in./ft)
$N(E)$	= describing function gain which is a nonlinear function of sinusoidal input amplitude E
PR	= Cooper-Harper pilot rating (Ref. 1)
$q[\ ]$	= quantization nonlinearity, Fig.9
s	= Laplace operator for differentiation
$T_{\dot{x}}$	= equivalent path mode time constant, s
X	= fore and aft position, ft
X_C	= commanded position, ft
δ_S	= pilot's stick position (positive stick aft, in.)
Δ_S	= modified stick position (positive stick forward, in.) $=-\delta_S$
θ	= body-axis pitch attitude, deg
ω_{LS}	= limit-cycle frequency

Introduction

ANALYSIS of control systems using man-in-the-flight-control-loop techniques has grown increasingly useful as a means of designing control systems to achieve desirable flying qualities.[2-4] Hess[2] and Ashkenas et al.[4] have used pilot models to investigate pilot-induced oscillations for various problematic flight vehicles. These methods recognize the importance of the often overlooked feedback loop closures implemented by the pilot. Pilot compensation, or lack of it, strongly influences the dynamic response properties of the man-in-the-loop vehicle.

This paper deals with a flight experiment in which the pilot behavior is pulsive or steplike. Pulsive behavior means that the pilot's stick moves rapidly from one position to another and then remains nearly stationary for some time. Pulsive pilot behavior has been observed by other researchers[2,5,6] when the pilot was controlling a plant of the form K/s^2. Furthermore, for plants of this type, the probability distribution of pilot stick amplitude tends to be bimodal.[5] This indicates that pilots for plants of this type have preference for certain stick amplitudes.

The research presented in this paper deals with a class of plants in which the X position of a hovering VTOL is being controlled by the pilot. Since the VTOL control system is a translational velocity command (TRC) control system, the controlled element is approximately

$$\frac{X(s)}{\Delta_S(s)}=\frac{K_{\dot{x}_c}}{S(T_{\dot{x}}S+1)}$$

where $T_{\dot{x}}$ is in the range from 1.3 to 3.7 s. The results presented here suggest that, for plants of this type, the pilot's behavior is pulsive. In addition, the probability distribution of stick deflection is bimodal. A simple nonlinear pilot model is described which duplicates many of the pilot properties observed in flight.

Flight-Test Data

This research is based upon an experiment flown by the X-22A variable stability VTOL aircraft.[7,8] Generic flying quality for aircraft with translational velocity command control systems was the primary objective of that experiment. The piloting task involved tracking a moving landing pad in the presence of unavoidable natural turbulence and synthetically generated and measured shipwake turbulence. Synthetic turbulence was generated to achieve a root mean square (rms) velocity of 8.9 ft/s in each of three orthogonal directions. Gaussian white noise was driven into a second-order transfer function which had a damping ratio of 0.4 and a natural frequency of 1.1 rad/s. Motion of the landing pad involved discrete jumps in either x, y, or x and y positions of ± 25 ft occurring approximately every 25-30 s in a semi-random manner. Landing pad position was presented to the pilot on a head-up display but the task was visual otherwise.

The objective of this paper is to study only the pilot's longitudinal behavior in hover. Although the pilot's flight task was more complex than longitudinal positioning, an effort was made in data selection to minimize the influence of lateral positioning, altitude control, and heading control on pilot behavior. In a typical scenario, the pilot, following a jump in landing pad position, would rapidly reposition over the pad and then precisely hover over the new pad position. It is this period of hover over a fixed landing pad in the presence of turbulence which is studied herein.

Presented as Paper 83-2232 at the AIAA Guidance and Control Conference. Gatlinburg, Tenn., Aug. 15-17, 1983; submitted Aug. 23, 1983; revision submitted March 26, 1984.

*Assistant Professor, School of Aeronautics and Astronautics. Member AIAA.
†Ph.D. Candidate.

A typical mathematical model for the X-22A is shown below for configuration 211B.

$$\begin{bmatrix} \dot{x} \\ \ddot{x} \\ \dot{\theta} \\ \ddot{\theta} \end{bmatrix} = \begin{bmatrix} 0 & 1 & 0 & 0 \\ 0 & -0.16 & -0.562 & -0.0614 \\ 0 & 0 & 0 & 1 \\ 0 & 11.9^* & -9.04 & -5.73 \end{bmatrix} \begin{bmatrix} x \\ \dot{x} \\ \theta \\ \dot{\theta} \end{bmatrix}$$

$$= \begin{bmatrix} 0 \\ 0 \\ 0 \\ \underline{-47.9} \end{bmatrix} \Delta_S$$

The number marked with the asterisk is proportional to the inertial velocity feedback gain of the X-22A which was adjusted between X-22A flight configuration to achieve different equivalent path mode time constants ($T_{\dot{x}}$). The number underlined is proportional to the stick gain and was adjusted between X-22A configuration to achieve different command path gains ($K_{\dot{x}_c}$). The transfer function for X per stick deflection for configuration 211B is

$$\frac{X(s)}{\Delta_S(s)} = \frac{2.9(S+9.2)}{S(S+3.5)(S^2+2(0.78)(1.5)S+1.5^2)}$$

Determination of the equivalent path mode time constant, $T_{\dot{x}}$, involves applying a step stick input and determining the time to reach 63% of the steady-state velocity response. For configuration 211B, $T_{\dot{x}} = 1.4$ s. This paper deals with X-22A configurations which differed from each other only by the two numbers mentioned above.

The pitch and roll axes of the X-22A were mechanized to give approximately the same dynamic response to pitch and roll stick deflection. Altitude and heading hold were mechanized in the altitude and yaw axes. The yaw degree of freedom was not considered a factor in the flight experiment.

A force-feel system on the X-22A was invariant throughout this flight experiment. It gave the pilot a second-order response of stick position to stick force which had a natural frequency of 12 rad/s, a damping ratio of six-tenths, and a stick force gradient of 2.5 lb/in. A force trim device allowed the pilot to eliminate trim forces without modification of stick position. As a result, stick position biases are not an indication of steady stick forces.

Measured Pilot Behavior

Figures 1-3 show examples of pilot activity following a jump in pad position, including the region of hover over the fixed pad. These configurations had different path mode time constants, command path gains, and natural wind environments as described in Table 1. Note that configuration 217C had no synthetic turbulence while all other table entries did.

The startling feature in these figures is the existence of a nearly constant amplitude oscillation in the X position, pitch attitude, and stick deflection. The persistent oscillation, typical of lightly damped closed-loop systems, is characterized by reasonably large amplitude. For example, the peak-to-peak pitch attitude is approximately 6, 8, and 10 deg for these three configurations. Table 2 summarizes the properties of the persistent oscillations for many different flight conditions.

Pilot commentary indicates that the pilot definitely is influenced by these oscillations. For the three configurations the pilot commented "having trouble holding position," "trouble stopping," and "the biggest problem was predicting the corrections to stop in the box." It is also noted that when the oscillation amplitude is smaller as in configuration 202D ($K_{\dot{x}_c} = 4.4$, $T_{\dot{x}} = 1.9$, peak-to-peak pitch attitude of 4 deg), the pilot commented "hover easy to perform." Correlation of peak-to-peak stick motion and normalized peak-to-peak displacement with pilot rating is shown in Fig. 4. The size of the boxes indicates the range of uncertainty in the measurement of the peak-to-peak motion. Note also that Cooper-Harper pilot ratings have a variability of ±1. Based on these results it is fair to conclude that the properties of the persistent oscillation strongly affect pilot rating and commentary.

On the assumption that the pilot will generate his stick deflection based on observations (at least in part) of his position, a phase-plane plot of stick deflection vs position is shown for two configurations in Figs. 5 and 6. Note that in these plots biases exist in both X position and stick so that the center of the region of activity is not zero on either axis. Figure 5 shows two strong trends:

1) An approximate proportionality exists between stick position and vehicle position.

2) Frequent periods exist when the stick is moved rapidly before the vehicle position has a chance to change. This

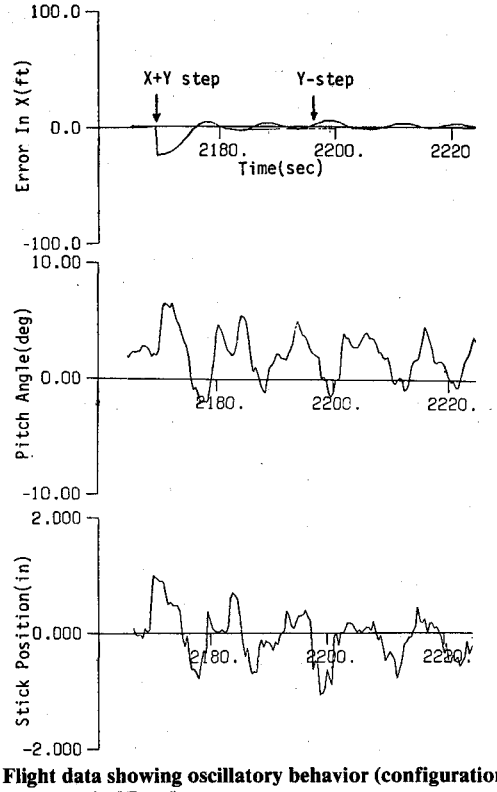

Fig. 1 Flight data showing oscillatory behavior (configuration 208B, $K_{\dot{x}_c} = 5.8$, $T_{\dot{x}} = 1.9$, PR = 4).

Table 1 Flight data characteristics (no synthetic turbulence)

Flight/ configuration no.	K_{x_c} ft/s/in.	$T_{\dot{x}}$, s	Cooper-Harper, PR	Steady winds, knots
211B	3.3	1.4	4.5	8
201F	2.9	1.9	6	"Smooth"
202D	4.4	1.9	2	"Smooth"
208B	5.8	1.9	4	5
206B	5.8	1.9	4	15-20[a]
207E	6.2	2.4	5.5	3-4
217C	8.5	2.8	5	10-15
206D	8.3	3.7	6	15-20[a]
207A	12	3.7	4.5	3-4

[a] X-22A duct tile angle = 80 deg.

Table 2 Flight-measured oscillation properties

Flight/ configuration no.	Resonant frequency, rad/s	Peak-to-peak				Loop[a] gain, 1/s
		X, ft	0, deg	δ_S, in.	δ_S/X, in./ft	
211B	1.1	3-4	7.9-8.7	1.6	0.45	1.5
201F	0.69-0.73	5-8	8.3-8.7	2.9-3.5	0.54	1.6
202D	0.8-0.94	3-5	4-4.7	0.5-0.8	0.16	0.70
208B	0.6-1.0	4-8	5.5-6.3	0.7-1.4	0.17	0.99
206B	0.7-0.8	6-9	8-9	1.0-1.8	0.19	1.1
207E	0.8-0.9	7-9	9-12	2.0-2.5	0.28	1.7
217C[b]	0.6-0.8	8-10	7.5-9.4	1.2-1.5	0.15	1.3
206D	0.6-0.8	7-12	–	–	–	–
207A	0.6-0.9	10-12	9-10	1.2-1.6	0.13	1.6

[a] Loop gain $= K_{x_c}$ (δ_S/X). [b] No synthetic turbulence.

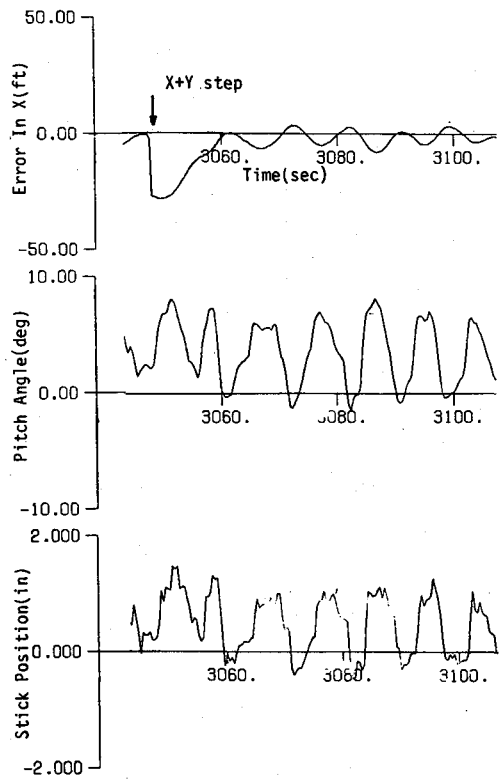

Fig. 2 Flight data showing oscillatory behavior on a configuration not driven by synthetic shipwake turbulence (configuration 217C, $K_{\dot{x}_c} = 8.5$, $T_{\dot{x}} = 2.8$, PR = 5).

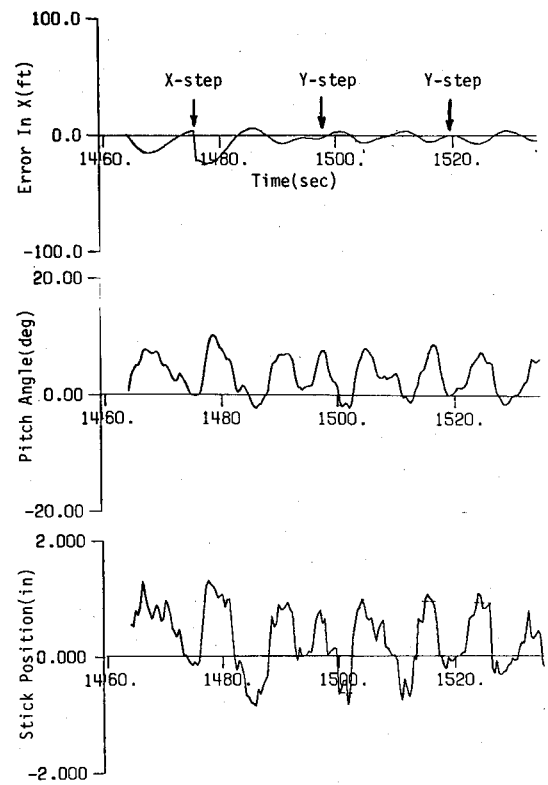

Fig. 3 Flight data showing oscillatory behavior (configuration 207A $K_{\dot{x}_c} = 12$, $T_{\dot{x}} = 3.7$).

corresponds to nearly vertical line segments on Fig. 5. On the average the vertical line segments cover approximately 0.25 in. of stick motion.

Figure 6 shows approximately the same information as Fig. 5 except that the curves are perhaps more elliptical. A possible explanation for the elliptical behavior of the phase-plane plot might be the presence of pilot velocity feedback. This may result because the configuration of Fig. 6 has a larger path mode time constant (the TRC system has lower velocity feedback gain).

One further observation can be made regarding stick activity. The pilot seems to prefer certain stick amplitudes. For example, in Fig. 1 the pilot seems to prefer stick positions of -0.4 ± 0.5 in., while in Figs. 2 and 3 he seems to prefer 0.5 ± 0.6 in. A histogram of stick behavior for configuration 220C is shown in Fig. 7. The figure indicates a distribution of stick activity which is approximately bimodal (-0.1 ± 0.2).

Linear Pilot Model Analysis

In this section, Figs. 5 and 6 are used to make inferences as to possible linear pilot models. Based on Fig. 5, a reasonable first approximation to this relationship between stick and X position is

$$\delta_S = K_x X$$

The pilot gain K_x can be estimated for configuration 211C ($K_{\dot{x}_c} = 9.4$, $T_{\dot{x}} = 1.4$) in the following manner. Table 2 indicates that for configuration 211B ($K_{\dot{x}_c} = 3.3$, $T_{\dot{x}} = 1.4$), the ratio of stick, to X peak-to-peak is 0.45 in./ft. Under the assumption that the pilot will adjust his gain to achieve the same value of $K_x K_{\dot{x}_c}$ in these two configurations, the value of K_x for configuration 211C is 0.16 in./ft. A straight line with slope of 0.16 (adjusted for measurement offsets in both X and δ_S) is a reasonable straight line approximation to the phase-

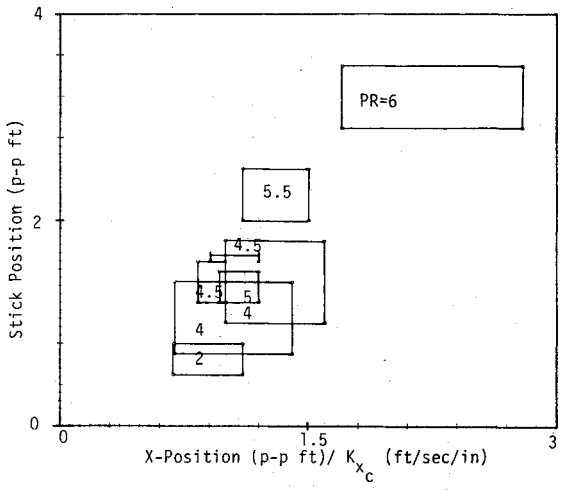

Fig. 4 Correlation of measured oscillatory motion properties with pilot rating.

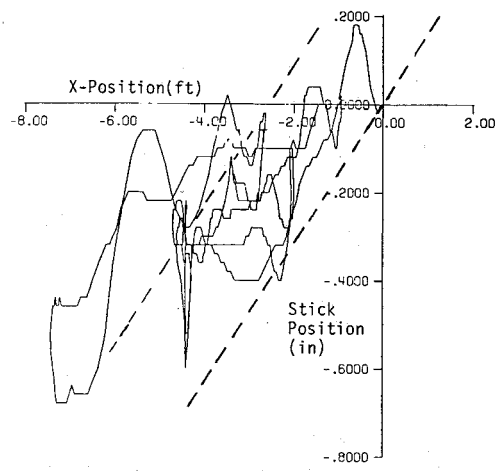

Fig. 5 Plot of stick deflection vs position showing stick quantization (configuration 211C, $K_{\dot{x}_c}=9.4$, $T_{\dot{x}}=1.4$, PR=4).

Table 3 Describing function properties

System transfer function:

$$\frac{X(S)}{\delta_S(S)}=\frac{a_1S+a_0}{S^4+b_3S^3+b_2S^2+b_1S}$$

Describing function for ideal relay with dead zone:

$$N(E)=\frac{4M}{\pi E}\left(1-\frac{A^2}{E^2}\right)^{1/2}$$

Limit-cycle frequency:

$$\omega_{LS}(b_1+ga_1)/b_3$$

$$g=(-R\pm\sqrt{S})/(2a_1^2)$$

$$R=2a_1b_1-a_1b_2b_3+a_0b_3^2$$

$$S=(a_0b_3^2-a_1b_2b_3)^2+4a_0a_1b_1b_3^2$$

Minimum gain for stable limit cycle:

$$K_x^*=\pi Ag/2M$$

Properties of minimum gain limit cycle:

$$E^*=\sqrt{2}A \text{ (in.)}$$

$$e_x^*=4\sqrt{2}M/\pi g=22E^*/K_x^* \text{ (Peak-to-peak, ft)}$$

plane plot of Fig. 5. Thus, configuration 211B of Table 2 is in reasonable agreement with Fig. 5 on pilot gain K_x.

Figure 8 shows a Bode plot for configuration 218E ($K_{\dot{x}_c}=7.6$, $T_{\dot{x}}=1.4$). Again keeping the product of K_x and $K_{\dot{x}_c}$ equal to that of configuration 211B gives a pilot gain of $K_x=0.2$ in./ft for configuration 218E. Adjusting the amplitude ratio in Fig. 8 for configuration 218E by -14 dB (20 log 0.2) indicates a gain crossover frequency of 1.1 rad/s. At this frequency the phase margin is about 12 deg, indicating lightly damped pilot-in-the-loop system behavior in the region of 1.1 rad/s. This agrees exactly with the resonant frequency of 1.1 rad/s observed in flight for configuration 211B (Table 2).

A similar analysis for configuration 206D ($K_{\dot{x}_c}=8.3$, $T_{\dot{x}}=3.7$) gives a pilot gain of 0.19 in./ft, a gain crossover frequency of 0.66 rad/s, and a phase margin of 5 deg. This analysis is based upon the flight measured pilot gain for configuration 207A ($K_{\dot{x}_c}=12$, $T_{\dot{x}}=3.7$) found in Table 2. A phase margin this small again suggests lightly damped pilot-in-the-loop system behavior in the region of 0.66 rad/s. Table 2 confirms that configuration 206D demonstrated resonance in the frequency range of 0.6-0.8 rad/s.

It can be concluded that the simple linear gain pilot model with pilot gain determined from flight is sufficiently accurate to predict the pilot-in-the-loop resonant frequency also observed in flight.

It is now possible to extend the pilot model to introduce the possibility of velocity feedback, i.e., a pilot model of the form

$$\delta_S=K_x(\tau\dot{X}+X)$$

If sinusoidal motion in position is assumed, i.e., $X=b\sin(wt)$, then the stick behavior will be

$$\delta_S=K_x\tau bw\cos(wt)+K_xb\sin(wt)$$

Phase-plane plots of δ_S vs x will be ellipses tilted to a slope of K_x. When $X=0$ (or halfway between peak-to-peak X in Fig. 6), the stick deflection should be $\pm K_x\tau bw$ (relative to the mean stick position in Fig. 6). This analysis gives us an indication of the pilot lead time constant. For configuration 207A of Fig. 6, a reasonable value of τ is 1.2 s based upon $w=0.66$ rad/s, $b=4$ ft, $K_x=0.13$ in./ft.

The effect of the addition of this much pilot lead time constant on configuration 206D of Fig. 8 moves the pilot-in-the-loop position mode poles from a damping ratio of 0.04 at a natural frequency of 0.67 to a damping ratio of 0.46 at a natural frequency of 0.84 rad/s. The resonance of the piloted system would have substantially reduced amplitude and a resonant frequency near 0.84 rad/s. This resonant frequency is within the range of experimental accuracy in determining the resonant frequency from flight (0.6-0.9) in Table 2. As a result of this ambiguity in the flight data, it is not possible at

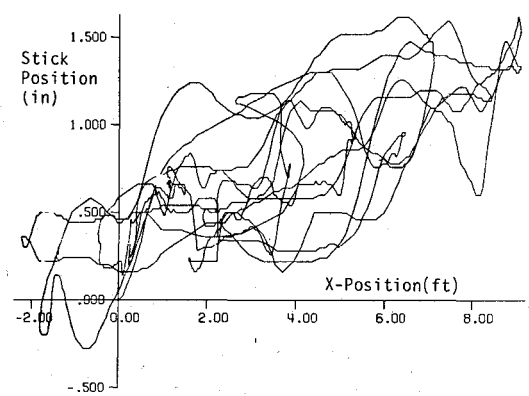

Fig. 6 Plot of stick deflection vs position showing stick quantization (configuration 207A, $K_{\dot{x}_c}=12$, $T_{\dot{x}}=3.7$, PR=4.5).

this point to argue conclusively either for or against this much velocity feedback.

We can assume that for the configuration with smaller path mode time constants (more velocity feedback in the TRC system) the pilot would use less velocity feedback. This is supported by Fig. 5. Thus, for the configuration studied in this paper, $\tau = 1.2$ s can be considered an approximate upper limit on pilot lead time constant.

It is interesting to note that for configuration 206D the crossover pilot model[5] would predict a pilot lead time constant approximately equal to the equivalent path mode time constant of 3.7 s. This much velocity feedback is not supported by either Fig. 6 or the resonant frequency observed in flight.

Based on this analysis, the following conclusions can be drawn:

1) For small path mode time constants ($T_{\dot{x}} = 1.4$ s) the pilot is employing only position feedback.

2) For larger path mode time constants ($T_{\dot{x}} = 3.7$ s) the pilot may or may not be using a lead time constant as large as 1.2 s. This is substantially smaller than would be predicted by the crossover pilot model.

Nonlinear Pilot Model

In this section the steplike behavior of the pilot's stick motion is modeled. Recall from the previous discussion of Figs. 5-7 that the pilot's stick seems to move in increments which vary between 0.25 and 0.6 in. This observation, together with the gross proportionality between stick displacement and vehicle position (described earlier in the section involving linear pilot modeling), allows a new nonlinear pilot model to be proposed as follows:

$$\delta_S = q[K_x(X - X_c)]$$

In this equation, $q[\ ]$ is the quantization nonlinearity defined in Fig. 9. K_x the pilot gain, and X_c the commanded x position (assumed to be zero). Figure 9 shows the pilot-in-the-loop system in block diagram form. Any velocity feedback generated by the pilot is not included in the quantized pilot model, an assumption which will require further justification.

Significant features of this quantized pilot model and the resulting pilot-in-the-loop system dynamics are:

1) For a range of pilot gains ($0.18 < K_x < 0.23$ for one configuration) the pilot-in-the-loop system exhibits persistent constant amplitude oscillations in the absence of any forcing function (i.e., limit cycles).

2) For lower gains, the system is asymptotically stable (neutrally stable in position when the stick reaches zero deflection because of the pole at the origin of the open-loop system).

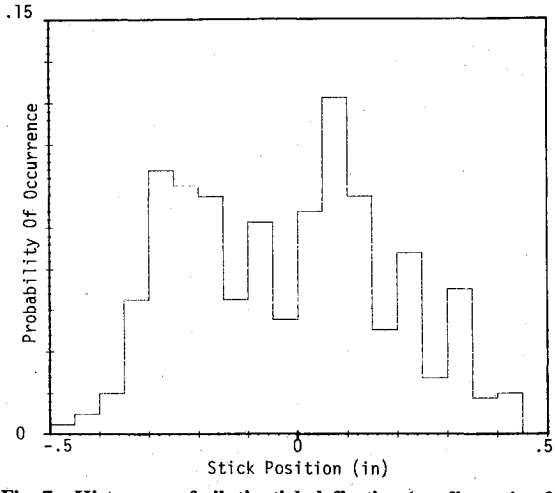

Fig. 7 Histogram of pilot's stick deflection (configuration 220C).

3) For gains higher than the range of gains for stable limit cycles the pilot-in-the-loop system in unstable.

4) When the stick deflection is small, i.e., +0.25, 0, and −0.25 in., the quantization nonlinearity dominates the response and the quantization nonlinearity can be modeled as an ideal relay with dead zone.

5) When the stick deflection is large, $|\delta_S| \gg 0.25$, the stick behavior is approximately linear and the system can be modeled as approximately linear with the control law $\delta_S \approx K_x(X - X_c)$.

In order to study the properties of this nonlinear closed-loop control system, the describing function (DF) method[9] will be used. This technique assumes sinusoidal motion throughout the nonlinear system. As its name implies, the DF is a quasilinear representation for a nonlinear element subjected to a sinusoidal input. The DF is defined as the complex ratio of the fundamental component of the output of the nonlinear element to the sinusoidal input.

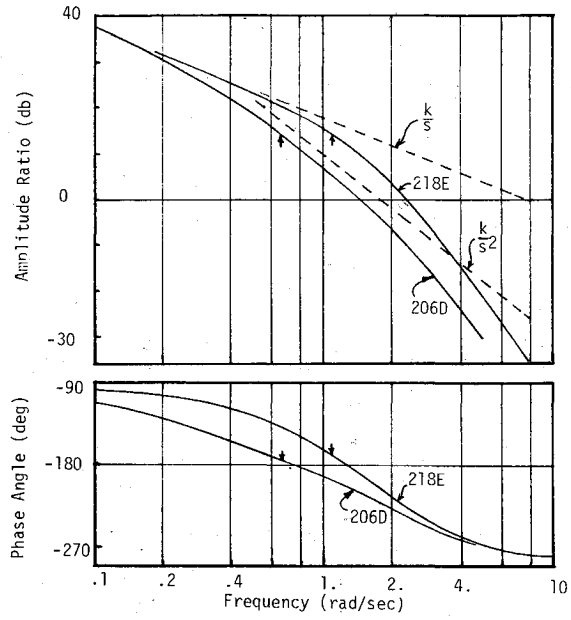

Fig. 8 Bode plot for X/Δ_S transfer function for configuration 218E ($K_{\dot{x}_c} = 7.6$, $T_{\dot{x}} = 1.4$) and configuration 206D ($K_{\dot{x}_c} = 8.3$, $T_{\dot{x}} = 1.4$).

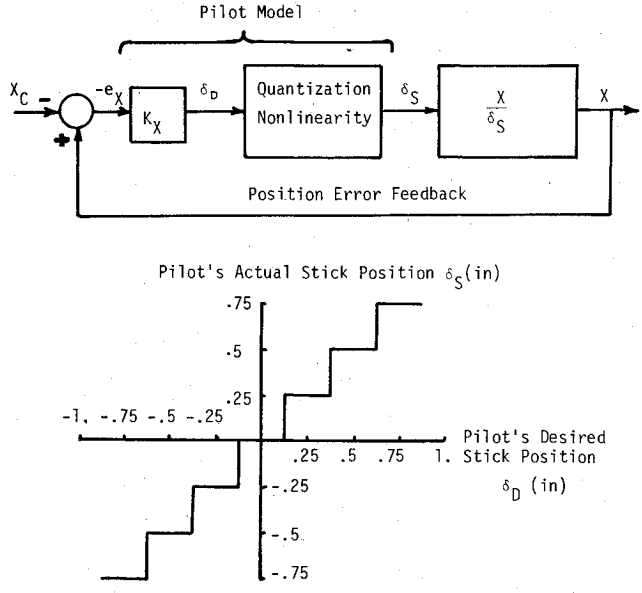

Fig. 9 Quantized pilot model: block diagram and unity slope quantizer.

When the quantized pilot model generates the smallest possible stick motion, stick deflections of +0.25, 0, and 0.25 in. result. This control policy can be modeled as a relay with dead zone. Since this type of nonlinearity does not change the phase relationship between the input and output waveforms, the DF is a real function, $N(E)$. When the input sinusoid has amplitude E, the output sinusoid has amplitude $N(E)$ and is in phase with the input where

$$N(E) = \frac{4M}{\pi E}\left(1 - \frac{A^2}{E^2}\right)^{1/2}$$

For the quantized pilot model proposed here, $M = 0.25$ in. and $A = 0.125$ in. Limit-cycle behavior can be induced by solving for "quantized pilot gain," $K_x N(E)$, so that the closed-loop system has poles on the stability boundary ($j\omega$ axis in the s plane). As noted, there exists a range of pilot gains which admit limit-cycle behavior. It seems reasonable to assume that the pilot might select the minimum gain for stable limit cycle, thereby, in a sense, maximizing his "gain margin" while minimizing his workload. The minimum pilot gain K_x^* occurs when $N(E)$ is a maximum and is a unique gain for this DF. A summary of the DF properties is given in Table 3.

Several very interesting properties of the limit cycle motion are described below.

1) The limit-cycle frequency ω_{LS} is independent of M or A of the relay and depends only upon the vehicle transfer function.

2) The minimum gain for stable limit cycle, K_x^*, always can be found and produces the smallest motion.

3) When we assume that the quantizer has a slope of one, i.e., $A = M/2$, the following additional observations can be made:

a) $K_x^* = \pi g/4$ and is independent of M or A. g is defined in Table 3 and is a function of the vehicle transfer function only.

b) $e_x^* = \sqrt{2}M/K_x^*$ is a linear function of M, where e_x^* is the amplitude of the position error in Fig. 9.

These properties are significant because the magnitude of the pilot's stick M may not be known prior to a flight experiment. However, as long as $A = M/2$ the limit-cycle frequency and minimum pilot gain are independent of M. M, however, does scale the magnitude of the resulting system response through property 3b above. (It should be noted that the DF method is an approximate method.) In the pilot modeling application, use of the describing function is extremely convenient since it provides a closed-form means of getting a reasonably accurate estimate of the actual limit-cycle properties.

Table 4 shows the computed limit-cycle frequency, minimum gain for stable limit cycle (K_x^*) computed analytically from the DF equations in Table 3. The flight conditions in the table correspond with those in Table 1. Note the excellent agreement between K_x^* in Table 4 and δ_S/X in Table 2. This comparison is shown in Fig. 10. It can be concluded that the quantized pilot model produces pilot gains which agree nicely with flight-measured pilot gains.

When analyzing the closed-loop system behavior, if the unity slope quantizer is ignored, then the resulting linear system can be analyzed in the conventional manner. Table 4 shows for this linear system (with pilot gain K_x^*) the time to half-amplitude of the lightly damped mode involving most strongly the position degree of freedom.

In order to get an idea of how well the quantized pilot model flies the X-22A, a closed-loop simulation was mechanized which utilized measured shipwake turbulence as an input. The simulation used K_x^* from the describing function analysis and the quantization nonlinearity (Fig. 9) with a step size of $M = 0.25$ and $A = 0.125$. The 40-s simulation used the same measured shipwake turbulence time history for all configurations. Typical simulation results are shown in Figs. 11 and 12 and Table 5.

The fact that the quantized pilot model leads to pilot-in-the-loop response amplitudes which agree well with flight data can be ascertained from Table 5 and Fig. 13. Furthermore, the fact that the peak-to-peak X-position amplitude (Fig. 13) is not overpredicted by the quantized pilot model is strong evidence that the closed-loop system has a realistic level of "damping" in the position mode. This strongly suggests that pilot velocity feedback, which was not modeled in the quantized pilot model, is not significant for the data analyzed.

Selection of the quantization increment at 0.25 in. was based upon Figs. 1-3 and 5-7 as discussed previously. However, there remains some uncertainty as to whether this value is appropriate, and to what extent the quantization increment affects the simulation results. The latter question can be answered by simulation of the quantized pilot-in-the-loop system using different quantization increments. Such

Table 4 Analytical properties of limit cycle and nonlinear pilot model determined using the describing function method

Flight/ configuration no.	Limit-cycle frequency, rad/s	Min. pilot gain, in./ft	$t^{1/2}$[a]
211B	1.7	0.44	8.6
201F	1.1	0.51	12.2
202D	1.1	0.34	12.2
208B	1.1	0.26	12.2
206B	1.1	0.26	12.2
207E	0.87	0.24	15.5
217C	0.73	0.18	18.3
206D	0.55	0.18	23.9
207A	0.55	0.13	23.9

[a] Time to one-half amplitude of the lightly damped position mode of the linear system with pilot gain K_x^*.

Table 5 Oscillatory motion properties using stochastic simulation and nonlinear pilot model

Flight/ configuration no.	Resonant frequency, rad/s	Peak-to-peak[a] X, ft	Peak-to-peak[a] ϕ, deg	Peak-to-peak[a] δ_S, in.
211B	1.1-1.2	3.1	7.5	1.4
201F	0.91-1.1	4.2	6.7	2.1
202D	0.91-1.2	4.6	7.4	1.6
208B	0.91-1.1	4.4	7.1	1.1
206B	0.91-1.1	4.4	7.1	1.1
207E	0.75-0.79	4.5	5.4	1.1
217C	0.69-0.78	7.2	7.4	1.3
206D	0.65-0.76	11.0	9.8	2.0
207A	0.61-0.70	11.9	10.6	1.6

[a] Peak-to-peak = 2.83 × rms.

Table 6 Comparison of unquantized vs quantized pilot models (configuration 208B) in the stochastic simulation

Quantization increment, in.	Pilot model gain, K_x, in./ft	Resonant frequency, rad/s	Peak-to-peak motion[a] X, in.	Peak-to-peak motion[a] ϕ, deg	Peak-to-peak motion[a] δ_S, in.
Flight data		0.6-1.0	4-8	5.5-6.3	0.7-1.4
0.25	0.256	0.91-1.1	4.4	7.1	1.1
0.35	0.256	0.91-1.3	4.7	7.5	1.2
0.50	0.256	0.96-1.2	5.4	8.9	1.5
0.75	0.256	0.92-1.1	6.4	10.6	1.7
0[b]	0.32[c]	1.0-1.2	6.9	13.3	2.2
0.25	0.32	1.0-1.2	7.5	14.8	2.4

[a] Peak-to-peak = 2.83 × rms. [b] This gain is the gain which produced a neutrally stable position mode at $\omega = 1.05$ rad/s. [c] Unquantized pilot model.

results are shown in Table 6 from which the following conclusions can be drawn:

1) Peak-to-peak motion amplitudes increase as the quantization increment increases but a 40% increase in quantization increment produces less than a 9% increase in closed-loop motion amplitude.

2) The response amplitudes for a quantization increment of 0.25 agree best with the flight data.

In the final analysis it appears that 0.25 in. is reasonable and the final answers are not particularly sensitive to this parameter. Table 6 also allows us to rule out a linear pilot model with position feedback sufficient to drive the position mode onto the stability boundary. Such a pilot model leads to response amplitudes too large by a factor of 2. Unfortunately, it is not possible to rule out a pilot model with some velocity feedback (which would reduce the vehicle response amplitudes) and with a greater quantization amplitude (which would increase response amplitudes).

Correlation with Flying Qualities

When asked to evaluate the flying qualities of a vehicle, the task description is of utmost importance to the pilot. In the X-22A experiment reported here, the relevant task initially involved large maneuvers to reposition over the new landing pad position following discrete pad motion and, second, precision hovering in turbulence. This paper studies only the precision hovering portion of the flight experiment and, as a result, offers only a partial explanation to the overall flying qualities evaluation provided by the pilot.

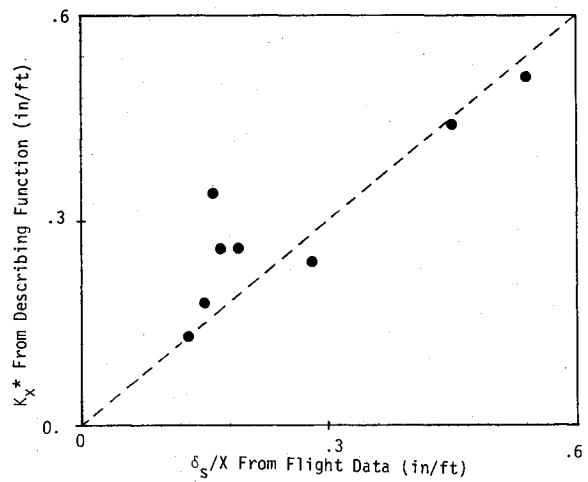

Fig. 10 Comparison of K_x^* from describing function analysis with δ_S/X obtained from flight data (in./ft).

Table 7

Property	Handling qualities parameter
σ_S (rms stick position)	Stick force comments
σ_x (rms X position)	Hovering performance
$AB=(\omega_{LS}/K_x^*)$	Abruptness

Table 8

Pilot comment	Simulation property
Stick forces undesirably light in.	$\sigma_S \leq 0.2$
Stick forces comfortable, in.	$0.2 < \sigma_S \leq 0.5$
Stick forces heavy, in.	$0.5 \leq \sigma_S 1$
Stick forces excessive, in.	$\sigma_S > 1$
Desirable vehicle performance, ft	$\sigma_X \leq 1.7$
Adequate vehicle performance, ft	$\sigma_X > 1.7$
Vehicle abrupt, ft/(s-in.)	$AB > 6$

The approach to flying qualities most often employed today involves analysis of specifications upon the open-loop vehicle without explicit concern for the pilot's loop closures. The open-loop specifications are designed, of course, to satisfy the pilot's expectations of the closed-loop vehicle's response. Difficulty is encountered, however, when the data base of desirable open-loop vehicles does not include the class of vehicles under design. In these cases, a pilot-in-the-loop analysis may reveal deficiencies in flying qualities which would not have been detected with the limited open-loop data base available or with limited flight data.

The quantized pilot model developed here provides a means of incorporating the final loop closure around the X-22A and evaluating the dynamic properties of the man-in-the-loop system, as well as overall system performance. This section will attempt to correlate closed-loop vehicle performance and pilot model parameters with handling qualities.

Using the describing function analytical procedure, the minimum pilot gain K_x^* was computed for 22 different configurations. With this gain and the quantizer removed, the eigenvalues of the resulting linear pilot-in-the-loop system were found. The lightly damped closed-loop position mode was found to have a time to one-half amplitude of 8-24 s for the configurations analyzed. It can be shown that the reciprocal of pilot gain and the time to one-half amplitude correlate strongly with open-loop velocity gain $K_{\dot{x}_c}$ and equivalent path mode time constant $T_{\dot{x}}$. Thus the open-loop handling qualities discriminators found to be useful in Ref. 7

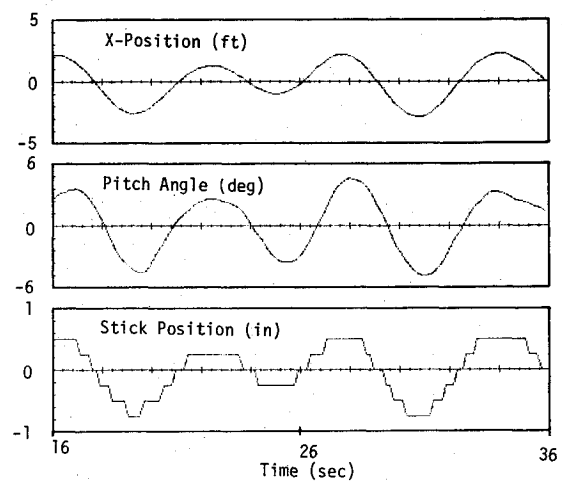

Fig. 11 Simulated data with quantized pilot model and shipwake turbulence input (configuration 208B).

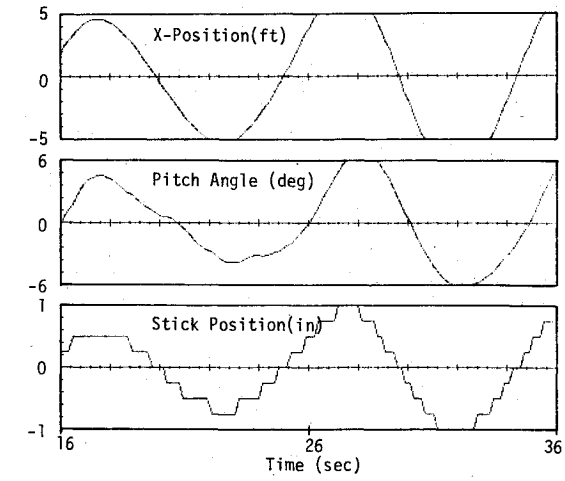

Fig. 12 Simulated data with quantized pilot model and shipwake turbulence input (configuration 207A).

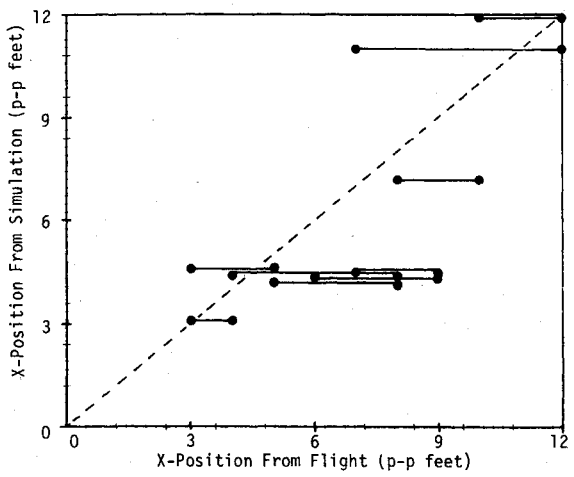

Fig. 13 Comparison of X position from stochastic simulation with flight data (peak-to-peak, ft).

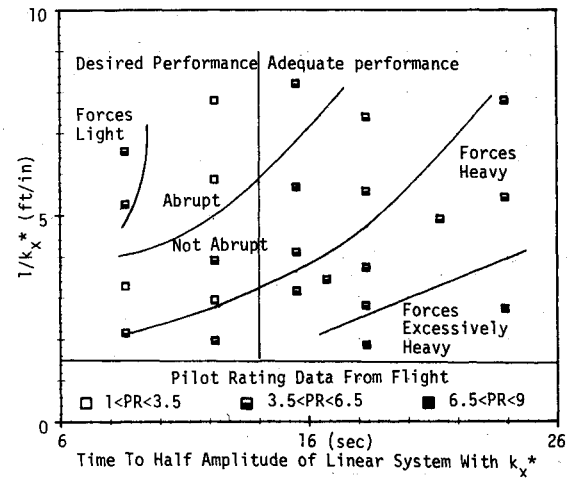

Fig. 14 Flying qualities characteristics obtained from stochastic simulation using quantized pilot model.

have their analogs in the pilot-in-the-loop parameters described above. Furthermore, by locating each configuration on a plot of $1/K_x^*$ vs time to one-half amplitude, regions of level 1, 2, and 3 flying qualities can be located. These regions, not surprisingly, correspond in shape to the regions found in Ref. 7. Figure 14 indicates level 1 flying qualities ($PR<3.5$) with an open square, level 2 ($3.5 \leq PR < 6.5$) with a half-full square, and level 3 ($PR > 6.5$) with a completely filled square.

Much more detailed and diagnostic information about handling qualities becomes available if the dynamic properties of the quantized pilot-in-the-loop system are compared with pilot commentary in Ref. 8. It is proposed that the following properties of the pilot-in-the-loop system correlate with handling qualities as shown in Table 7.

Based upon comparison of the properties listed in Table 7 (computed using the quantized pilot model driven by synthetic turbulence) with pilot commentary obtained from flight, the correlations listed in Table 8 were found and plotted on Fig. 14.

The results found in Table 8 are useful to the control system designer because, from dynamic simulation alone, it is possible to not only predict the level of flying qualities for a given vehicle but also to predict pilot commentary. This is diagnostic in that the designer can use the analytically predicted pilot commentary to help improve the vehicle control system.

Conclusions

A simple but nonlinear pilot model has been proposed for the precision hovering task of a VTOL with Translational Velocity Command control systems. The pilot model consists of one feedback gain on position error and a quantization nonlinearity on the pilot's stick positioning. Using this model, a pilot gain can be computed analytically which agrees remarkably well with flight measurements. The resulting oscillatory motion also agrees well with flight measurements. Closed-loop flying quality parameters (i.e., vehicle precision positioning performance, abruptness, and stick forces) have been computed numerically from simulation. These are shown to agree reasonably well with pilot commentary. The method of pilot-in-the-loop analysis is shown to lead to greater insight into why specific configurations generate specific pilot comments and shows the complex interrelationship between various handling quality factors.

Acknowledgments

The work reported herein was accomplished for the Naval Air Development Center under Contract N622-69-81-C-0729, with John W. Clark Jr. as Contract Technical Monitor. The authors also acknowledge the technical assistance provided generously by the Calspan Advanced Technology Center.

References

[1] Cooper, G.E. and Harper, R.P.H. Jr., "The Use of Pilot Rating in the Evaluation of Aircraft Handling Qualities," NASA TN D-5153, 1969.

[2] Hess, R.A., "Rationale for Human Operator Pulsive Control Behavior," *Journal of Guidance and Control,* Vol. 2, May-June 1979, pp. 221-227.

[3] Schmidt, D.K., "Optimal Flight Control Synthesis via Pilot Modeling," *Journal of Guidance and Control,* Vol. 2, July-Aug. 1979, pp. 308-312.

[4] Ashkenas, I.L., Hoh, R.H., and Teper, G.L., "Analyses of Shuttle Orbiter Approach and Landing," *Proceedings of the AIAA Guidance and Control Conference,* San Diego, Calif., 1982, pp. 810-820.

[5] McRuer, D.T. and Krendel, E.S., "Mathematical Models of Human Pilot Behavior," AGARDograph 188, Jan. 1974.

[6] Young, L.R. and Meiry, J.L., "Bang-Bang Aspects of Manual Control in High-Order Systems," *IEEE Translations on Automatic Control,* July 1965, pp. 336-341.

[7] Radford, R.C., Andrisani, D., and Beilman, J.L., "An Experimental Investigation of VTOL Flying Qualities Requirements for Shipboard Landings," NADC-77318-60, Aug. 1981.

[8] Radford, R.C. and Andrisani, D., "An Experimental Investigation of VTOL Flying Qualities Requirements in Shipboard Landings," *Journal of Aircraft,* Vol. 21, June 1984, pp. 371-379.

[9] Atherton, D.P., *Nonlienar Control Engineering,* Van Nostrand Reinhold Co., New York, 1975.